IEEE Access
Multidisciplinary ⋮ Rapid Review ⋮ Open Access Journal

Received December 17, 2019, accepted December 31, 2019, date of publication January 10, 2020, date of current version January 17, 2020.

Digital Object Identifier 10.1109/ACCESS.2020.2965584

Novel Unmanned Aerial Vehicle-Based Line-of-Sight MIMO Configuration Independent of Transmitted Distance Using Millimeter Wave

NAOKI MATSUMURA[1], (Student Member, IEEE), KENTARO NISHIMORI[1], (Member, IEEE), RYOTARO TANIGUCHI[1], (Student Member, IEEE), TAKEFUMI HIRAGURI[2], (Member, IEEE), TAKASHI TOMURA[3], (Member, IEEE), AND JIRO HIROKAWA[3], (Fellow, IEEE)

[1]Graduate School of Science and Technology, Niigata University, Niigata 950-2181, Japan
[2]Faculty of Fundamental Engineering, Nippon Institute of Technology, Saitama 345-8501, Japan
[3]Department of Electrical and Electronic Engineering, Tokyo Institute of Technology, Tokyo 152-8550, Japan

Corresponding author: Naoki Matsumura (nmatsumura@gis.ie.niigata-u.ac.jp)

This work was supported in part by SCOPE under Grant 165004002 and Grant 185004002, in part by the KAKENHI, Grant-in-Aid for Scientific Research (B) under Grant 17H01738 and Grant 17H03262, and in part by the Adaptable and Seamless Technology Transfer Program through Target-Driven R&D (A-STEP) from Japan Science and Technology Agency (JST) under Grant JPMJTM19F3.

ABSTRACT Recently, the millimeter-wave band has been used in outdoor wireless communications to improve the frequency utilization efficiency. In this study, we propose a method to realize line-of-sight multiple-input multiple-output (LOS-MIMO) transmission independent of the transmitted distance using a two-dimensional (2-D) fixed antenna element arrangement, assuming millimeter-wave-band communication by small autonomous unmanned aerial vehicles. In conventional LOS-MIMO transmission with uniformly spaced antenna elements, the theoretical upper bound of the channel capacity is obtained, which decreases at a certain transmitted distance. Therefore, we focus on the fact that the propagation channel characteristics in pure LOS are geometrically determined by the transmitted distance, and consider the optimization of the arrangement of antenna elements. The element arrangement is fixed without using antenna selection from the viewpoint of system simplification. In addition, from the viewpoint of array size, we study the optimization corresponding to a 2-D element arrangement. The proposed method approximates the optimal arrangement from a vast number of 2-D element arrangements using a genetic algorithm. We evaluate the channel capacity characteristics of the proposed method by computer simulation and show that the characteristic degradation due to change in the transmitted distance in conventional LOS-MIMO transmission is improved. In addition, we evaluate a 4×4 MIMO transmission in an outdoor environment. The 4×4 MIMO propagation channel is also measured by an actual measurement equipment in the 66-GHz band and it is shown that the measured and calculated results agree with each other.

INDEX TERMS Millimeter wave, unmanned aerial vehicle, line-of-sight multiple-input multiple-output, non-uniform antenna array, genetic algorithm.

I. INTRODUCTION

Recently, with the diversification of wireless communications, such as the Internet of Things (IoT), the fifth generation mobile communication (5G) system is targeted to increase the capacity of mobile data by more than 1000 times in comparison with that of 4G [1]. In the 5G system, the use of the microwave bands and the millimeter-wave bands has been studied with the aim of improving the utilization efficiency in limited frequency bands [1]. Under these circumstances, line-of-sight multiple-input multiple-output (LOS-MIMO) and orbital angular momentum (OAM) transmission have attracted much attention in order to realize millimeter-wave-band high-speed transmission in fixed wireless communications [2]–[7]. Although the principles of LOS-MIMO and OAM are different, the concepts are the same, and

The associate editor coordinating the review of this manuscript and approving it for publication was Hayder Al-Hraishawi.

space-division multiplexing is realized by geometrically optimizing the antenna design in the LOS environment. This is different from conventional MIMO transmission, which is effective in a rich multipath environment that assumes independent identically distributed (i.i.d.) Rayleigh fading between transmission and reception [8]–[10]. LOS-MIMO and OAM are expected to be used for wireless fronthaul/backhaul in next-generation mobile communications because they can achieve space-division multiplexing while achieving high signal-to-noise ratio (SNR) by utilizing the LOS environment [6], [11].

As communication traffic increases, the use of small autonomous unmanned aerial vehicles (UAVs) is attracting attention [12]. Experimental evaluation reports that when a UAV flying over buildings communicates with base stations using microwaves, the propagation loss approaches the square of the transmitted distance in proportion to the flight altitude [13]. According to the conventional propagation model, the propagation loss increases in proportion to the 3rd–4th power of the transmitted distance in an outdoor environment, assuming it is an urban area [14]. Therefore, high-speed transmission can be realized using UAVs. In fact, recently, there has been significant research on the realization of high-efficiency beam forming methods and stable networks when using millimeter-wave bands for communication via UAVs [15], [16].

In this study, we focus on the effectiveness of millimeter-wave bands in LOS-MIMO transmission and the possibility of LOS propagation by UAVs, and study millimeter-wave LOS-MIMO transmission using UAVs. The main issues when configuring a LOS-MIMO antenna for UAVs are: 1) robustness to changes in transmitted distance; 2) misalignment from the opposite position of the transmitter/receiver antenna; and 3) specific hardware. These items are indispensable for system realization. In this study, we focus on the solution of the first issue, which is an issue unique to UAVs. In conventional LOS-MIMO transmission, the spacing between adjacent elements in the array uses a uniformly spaced arrangement that is optimized for fixed wireless communications. Since the element spacing is optimal only for a certain transmitted distance, the rank of the propagation channel matrix is deficient due to the change in the transmitted distance [2], [3]. In this paper, we study the non-uniform arrangement of elements and improve the rank deficiency of the propagation channel matrix by making the difference in transmission length of each element distinct.

Non-uniform spacing for LOS-MIMO transmission has been used in certain studies. The optimization of non-uniform linear arrays has been investigated for the purpose of increasing the transmitted distance that can be spatially multiplexed [17], [18]. Reference [19] proposes a method that mechanically moves the position of some internal elements of the square array according to the transmitted distance. The array size constraint by the linear array and the method of mechanically moving the element position are difficult to implement in a system using UAVs. For the same reason, this study does not consider the use of OAM transmission. When OAM multiplex transmission using multiple phase modes is used, the issue of robustness to changes in transmitted distance can be expected to be solved by combining appropriate modes [7]. However, in the case of OAM multiplexing, a massive single array or multiple subarrays are used, and the system scale is expected to increase. Furthermore, dynamic mode selection according to the transmitted distance is also required. For this reason, we focus on LOS-MIMO, which has the possibility of a simpler antenna system than OAM multiplexing. In this study, we evaluate the characteristics when all the elements of the array are arranged in a square in a fixed manner. Reference [18] also mentions the case of a two-dimensional (2-D) array configuration. However, it differs from that used in this study because the water-pouring theorem is applied, and the aim is to improve the upper bound of the effective transmitted distance that occurs in a uniform arrangement.

When antennas are arranged within a certain range, the number of combinations becomes enormous and it is difficult to derive the exact optimal arrangement. Therefore, we study a method that approximates the optimal arrangement, and efficiently determines a more effective arrangement than conventional uniform spacing. We use a genetic algorithm (GA) [20] that is effective in deriving the approximate optimal solution, and realize an arrangement with a small amount of channel capacity degradation with changes in transmitted distance using fixed elements. Previous studies have confirmed the effectiveness of using GAs for antenna configuration. By using a GA for sector antenna configuration, the combination of multiple parameters, such as beam width and antenna gain, can be optimized [21]. We evaluate the characteristics of the approximate optimal arrangement derived by GA using computer simulation. In addition, we perform 4×4 MIMO transmission in an actual outdoor environment in the 66-GHz band and it is shown that the results calculated with the proposed method agree well with the measured results.

The remainder of this paper is organized as follows. Section II presents the target scenario of this study, and discusses the issues in conventional LOS-MIMO transmission and proposals for solving these issues. Section III shows the evaluation method for element arrangement using a GA. In Section IV, the channel capacity is calculated by computer simulation and the characteristics of the proposed method are evaluated. Section V confirms the effectiveness of using a non-uniform arrangement in 4×4 LOS-MIMO by actual transmission in an outdoor environment.

II. OVERVIEW, ISSUES AND PROPOSALS OF LOS-MIMO TRANSMISSION USING UNMANNED AERIAL VEHICLES

A. TARGET SCENARIO

The authors have studied MIMO transmission using UAVs in a LOS environment [24]. This paper contributes to the realization of applications such as those shown in Fig. 1 by proposing a new LOS-MIMO system that is independent of

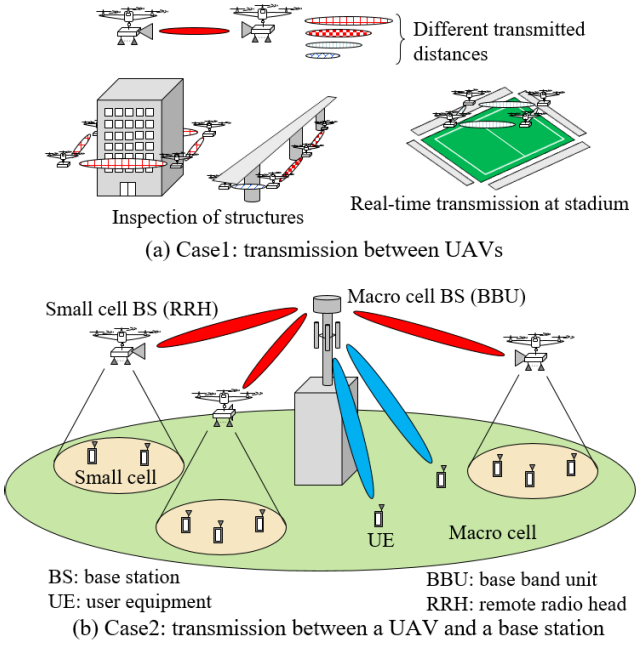

FIGURE 1. Application examples of LOS-MIMO system independent of transmitted distance.

the transmitted distance by using fixed elements. Fig. 1(a) is an example of applying millimeter-wave LOS-MIMO transmission when using UAVs for inspection of structures or real-time transmission at a stadium. By adapting to changes in transmitted distances, large-capacity transmission is expected regardless of the shape of the structure or stadium. Fig. 1(b) shows an example in which millimeter-wave LOS-MIMO transmission is applied to communication between a base station and a UAV. The UAV is used as a small cell base station for centralized-radio access network (C-RAN). C-RAN is used for next-generation mobile communications, including 5G system [1]. By adopting a UAV for remote radio head (RRH) and using millimeter-wave LOS-MIMO transmission in the front hall between the macro cell base station and the UAV, the small cell is dynamically configured according to the hot-spot. This is a new system, which is different from the conventional C-RAN.

B. OVERVIEW OF LOS-MIMO TRANSMISSION

Fig. 2 shows a model of LOS-MIMO transmission handled in this study. The transmitter and receiver have identical M-element antenna arrays facing each other in parallel. There is a pure LOS environment between the two arrays. The locations of the jth transmitting antenna and the ith receiving antenna are expressed as $\boldsymbol{S}_{Tx,j} = (x_{Tx,j}, y_{Tx,j}, 0)$ and $\boldsymbol{S}_{Rx,i} = (x_{Rx,i}, y_{Rx,i}, D)$, respectively, where D is the vertical distance between the facing arrays. The propagation channel between the two arrays can be written as [2]

$$\boldsymbol{H} = \begin{bmatrix} e^{-jkr_{11}} & e^{-jkr_{12}} & \cdots & e^{-jkr_{1M}} \\ e^{-jkr_{21}} & \ddots & & \vdots \\ \vdots & & & \\ e^{-jkr_{M1}} & \cdots & & e^{-jkr_{MM}} \end{bmatrix} \tag{1}$$

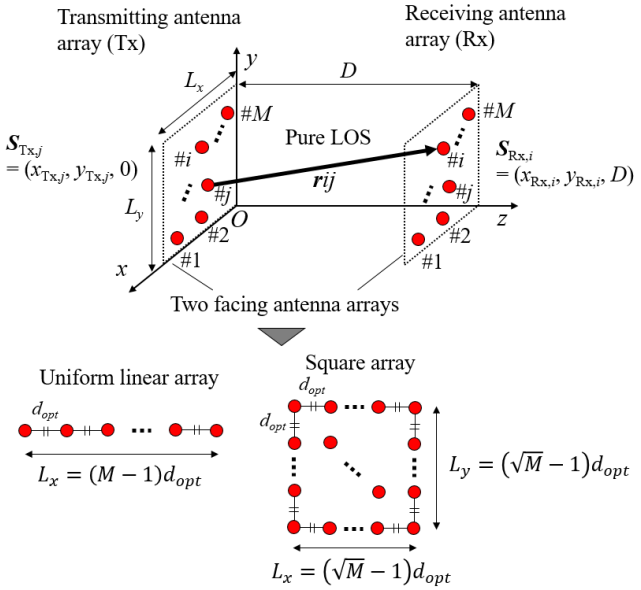

FIGURE 2. Conceptual diagram of LOS-MIMO transmission.

with

$$r_{ij} = \sqrt{\left(x_{Rx,i} - x_{Tx,j}\right)^2 + \left(y_{Rx,i} - y_{Tx,j}\right)^2 + D^2}, \tag{2}$$

where k is the wave number, which is defined as $k = 2\pi/\lambda_0$ with the free space wavelength λ_0 [m].

A LOS-MIMO system with uniform arrays orthogonalizes the propagation channel by setting the antenna element spacing d to the optimum value d_{opt} according to the transmitted distance D [m]. As a result, the system directly transmits the stream between the transmitting and receiving elements facing each other. The optimal element spacing for uniform arrays can be expressed as [3]

$$d_{opt} = \sqrt{\frac{D\lambda_0}{M_0}}, \tag{3}$$

where $M_0 \in \mathbb{Z}$ is the number of elements. In (3), $M_0 = M$ for an M-element uniform linear array (ULA), and $M_0 = \sqrt{M}$ for an M-element square array (SA). The propagation channel is orthogonalized by optimizing the difference in transmission length with the element spacing given by (3). The reason for this is shown by considering a 2 × 2 MIMO with a ULA as an example. From (1), the propagation channel matrix is written as

$$\boldsymbol{H} = \begin{bmatrix} e^{-jkr_{11}} & e^{-jkr_{12}} \\ e^{-jkr_{21}} & e^{-jkr_{22}} \end{bmatrix}. \tag{4}$$

From (4), the correlation matrix of the propagation channel matrix $\boldsymbol{Rr}$ is written as

$$\begin{aligned} \boldsymbol{Rr} &= \boldsymbol{H}\boldsymbol{H}^H \\ &= \begin{bmatrix} 2 & e^{-jk(R-D)} + e^{-jk(R-D)} \\ e^{-jk(R-D)} + e^{jk(R-D)} & 2 \end{bmatrix}, \end{aligned} \tag{5}$$

where $D = r_{11} = r_{22}$; and $R = r_{12} = r_{21}$. From (5), the conditions for $\boldsymbol{H}\boldsymbol{H}^H = 2\boldsymbol{I}$ ($\boldsymbol{I}$ is the unit matrix), where the propagation channel is orthogonal, are written as

$$|R - D| = (2p + 1)\frac{\lambda_0}{4}, \tag{6}$$

where $p \in \mathbb{Z}$. Therefore, considering that $d \ll D, R$, the element spacing of (3) satisfies (6). References [2] and [3] clarify that the propagation channels are orthogonal due to the same relationship by giving the element spacing according to (3) even in the case of $M \times M$ MIMO.

C. ISSUES AND PROPOSALS FOR LOS-MIMO TRANSMISSION

From (6), LOS-MIMO transmission achieves maximum performance when the difference in transmission length is an odd multiple of 1/4 wavelength. On the other hand, the system obtains the minimum characteristics when the transmitted distance changes and the difference in transmission length is an even multiple of 1/4 wavelength. Previous studies have used non-uniform array arrangements as a solution to this issue [17], [18]. Here, using the simplest three-element linear array as an example, we introduce the effectiveness of non-uniform arrangement. ULA and non-ULA models use the design shown in Fig. 2. The ULA element spacing d_{opt} is given by (3) with a frequency of 66.5 GHz and $D = 100$ m. Non-ULA is a non-uniform arrangement. In the non-ULA element spacing, the spacing between #1-#3 is $2d_{opt}$, and the spacing ratio between #1-#2 and #2-#3 is 0.6 : 0.4. The channel capacities of the ULA and the non-ULA were analyzed using eigenmode transmission. The channel capacity of eigenmode transmission is defined as [25]

$$C = \sum_{m}^{M} \log_2\left(1 + \lambda_m \frac{\gamma_0}{M}\right), \tag{7}$$

where γ_0 is the SNR and λ_m is the eigenvalue of the propagation channel matrix. The SNR was set with 10 dB as the reference at $D = 100$ m, and was assigned a distance attenuation proportional to the square of the transmitted distance. The number of transmission streams and the number of transmission antennas were the same. Fig. 3(a) shows the channel capacity versus the transmitted distance for the ULA and the non-ULA obtained by computer simulation. The upper bound gives the theoretical upper bound at which all the eigenvalues are constant [25]. The characteristics of ULA periodically reach the local maximum and minimum values. In this study, we describe this phenomenon as a periodic drop in the characteristics. In contrast to the ULA, the non-ULA supplements local minimum values everywhere. Fig. 3(b) shows the difference in transmission length distribution of the non-opposing elements in the ULA and the non-ULA receiving elements when $D = 33.3$ and 100 m. The difference in transmission length is normalized by the free-space wavelength. For the ULA, when $D = 33.3$ m, the differences in the transmission lengths of non-opposing elements of all elements are even multiples of 1/4 wavelength, which satisfy

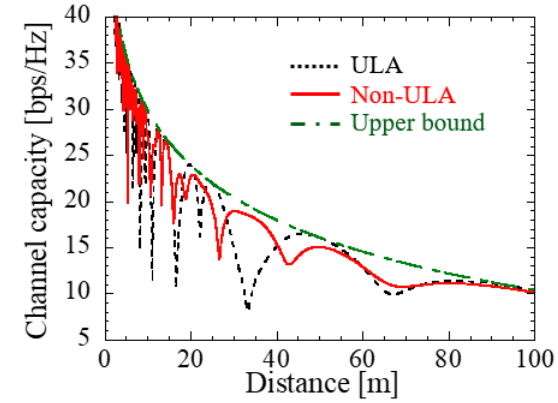

(a) Channel capacity versus transmitted distance

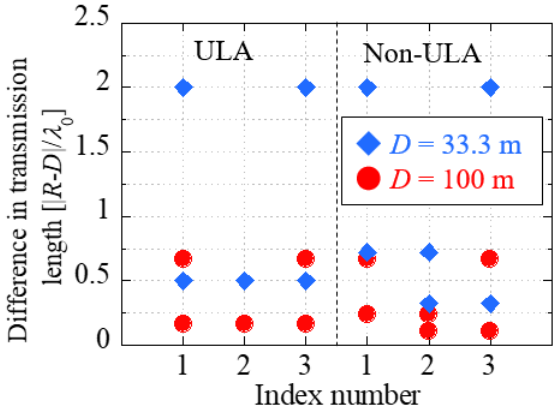

(b) Distribution of difference in transmission length

FIGURE 3. Comparison of three-element ULA and non-ULA.

the worst-case condition. On the other hand, for the non-ULA, when $D = 33.3$ m, the differences in the transmission lengths of more than half of all non-opposing elements are not even multiple of 1/4 wavelength. Therefore, a method that eliminates regularity from regular intervals in the conventional LOS-MIMO transmission is effective in constructing a system that is resistant to changes in the transmitted distance.

Using the characteristics of a non-uniform arrangement, we realize the construction of a system that compensates for the drop in channel capacity characteristics by arranging all elements in a fixed square. Fig. 3(a) shows that even with non-ULA, the characteristics drop at certain points when using fixed elements, as in the case of ULA. This is because when elements are fixed, the difference in transmission length physically transitions linearly with respect to changes in the transmitted distance. In other words, even with a non-uniform arrangement, the characteristics change greatly depending on the arrangement. To optimize the difference in transmission length in a 2-D plane, there are a large number of combinations of element arrangements. Therefore, we propose the derivation of the approximate optimal solution of the fixed element arrangement using a GA.

III. EVALUATION METHOD OF ANTENNA ARRANGEMENT USING GA

A. OVERVIEW OF GA

GA is one of the evolutionary computation methods. It is a search method that finds the optimal solution using accidental events based on biological evolution [20], [22]. Each generation has one population with an arbitrary number of individuals. The optimal solution is determined approximately by repeating the procedure of applying genetic operators to each individual of the population and handing over the new population to the next generation until a predetermined finish condition is reached. Typical optimal solution search methods include a random search that randomly extracts solutions from all solutions and evaluates them, and a steepest gradient method that searches for a better state from the current solution state. GA is a method that has the advantages of both methods by applying its genetic operator.

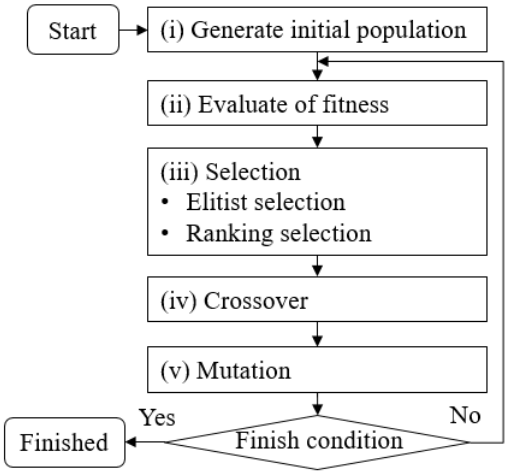

FIGURE 4. GA simulation flow.

B. EVALUATION METHOD

Under the assumption that the solution derived by GA is an approximate optimal solution, we verify that the non-uniform arrangement is more effective than the uniform arrangement. Fig. 4 shows the GA simulation flow used in this study. We use a basic GA that evaluates each individual by fitness, and searches by genetic operators such as selection, crossover, and mutation.

1) INITIAL SETTING

Information common to all individuals in the first-generation population, as well as information specific to an individual, is set. The common information includes transmitted power, frequency, number of elements, range of element arrangement, and transmitted distance. The information specific to each individual is the position of the elements and the channel capacity with respect to the transmitted distance. In summary, the individuals in this evaluation are the models in Fig. 2 configured by any element arrangement. The number of individuals in the population is always N.

2) FITNESS EVALUATION

The fitness is the evaluation index for each individual, and the goal is to maximize the following expression:

$$f_i = \mu_i - \sigma_i \tag{8}$$

with

$$\mu_i = \frac{1}{Q}\sum_{q=1}^{Q} C_{i,q} \tag{9}$$

and

$$\sigma_i = \sqrt{\frac{1}{Q}\sum_{q=1}^{Q}\left(C_{i,q} - \mu_i\right)^2}, \tag{10}$$

where μ_i is the mean value of the channel capacity for each transmitted distance $\{D_q \mid q = 1, 2, \ldots, Q\}$ calculated by (7) in the arrangement of individuals $i \in \mathbb{N}$; and σ_i is the standard deviation of the channel capacity according to $\{D_q\}$. As shown in Fig. 3, there is a theoretical upper bound for the channel capacity. The characteristics when evaluated over the entire transmitted distance are improved by searching such that the mean value of the channel capacity increases toward the theoretical upper bound. However, some of the local minimum values of the characteristics of each transmitted distance fall significantly from the mean value, e.g., $D = 33.3$ m in the ULA in Fig. 3(a). Therefore, the robustness of the change in the transmitted distance is evaluated by taking the value obtained by subtracting the standard deviation representing the degree of drop from the mean value as the fitness.

3) SELECTION

Each individual is sorted in descending order based on the fitness, and a selection is made using Baker's linear ranking selection [23]. In addition, the maximum value of the fitness is monotonically increased by using it in combination with the elite selection [22]. This increases the guarantee of the solution, because the finish condition of the algorithm in this study is that the number of generations reaches G.

4) CROSSOVER

Two selected individuals cross over according to the predetermined crossover rate p_c. Fig. 5(a) is an example of crossover for the case of four elements. One element from parents A and B is selected at random, and they are replaced to generate children Ab and Ba.

5) MUTATION

All individuals except those selected by elite selection mutate according to the mutation rate p_m. As shown in Fig. 5(b), one element randomly selected from the elements of the target individual moves to a random position.

The algorithm finish condition is when operations 2–5 above reach the prescribed number of generations. The individual with the highest fitness of the final generation is determined as an approximate optimal solution.

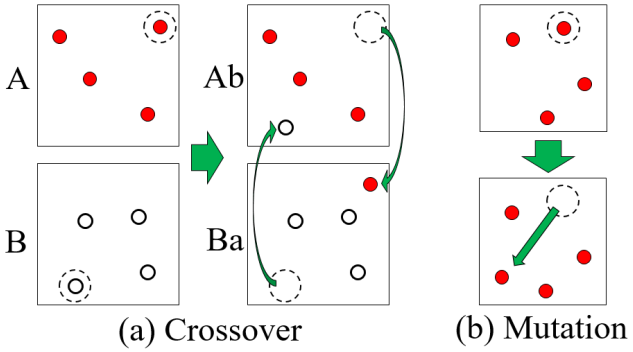

FIGURE 5. Examples of crossover and mutation in four-element arrangement.

IV. EVALUATION BY COMPUTER SIMULATIONS

A. CALCULATION CONDITIONS

The simulation model is the same as that shown in Fig. 2. M vertical omnidirectional antenna elements are arranged in a certain range with a square as a reference. In order to assume that pseudo-square arrangement is possible regardless of the number of elements, we defined the range of element arrangement based on (3) as

$$L = \sqrt{\frac{D\lambda_0}{\sqrt{M}}}\left(\sqrt{M}-1\right), \tag{11}$$

where L is the length of one side of the square, and the feedpoint of the element is placed in the $L \times L$ square. The same element arrangement was used on both the transmitting side (Tx) and the receiving side (Rx), and the mutual coupling between the elements was ignored. With Tx and Rx facing each other, Rx moved while Tx was fixed, and the characteristics at each transmitted distance were evaluated. The frequency was 66.5 GHz. The propagation channel matrix was a pure LOS environment, i.e., only direct waves existed. Digital control using eigenmode transmission was used for signal processing. For characterization, we calculated the channel capacity using (7). Furthermore, we calculated the mean value of the spatial correlations between the elements to comprehensively evaluate the influence of the difference in transmission length of all elements. Because the model has the same array configuration for both transmission and reception, we evaluated the receiving side correlation here. The equation for calculating the spatial correlation is written as

$$\begin{aligned}\rho &= \frac{1}{{}_M\mathrm{C}_2}\sum_{\{(a,b)|a\in A,b\in B,a>b\}}\frac{Rr_{ab}}{\sqrt{Rr_{aa}}\sqrt{Rr_{bb}}}\\ &= \frac{1}{{}_M\mathrm{C}_2}\sum_{\{(a,b)|a\in A,b\in B,a>b\}}\frac{\left|\sum_m^M h_{am}h_{bm}^*\right|}{\sqrt{\sum_m^M |h_{am}|^2}\sqrt{\sum_m^M |h_{bm}|^2}},\end{aligned} \tag{12}$$

where $A = \{2, 3, \ldots, M\}$ and $B = \{1, 2, \ldots, M-1\}$.

The comparison targets of the simulation were the proposed method (Prop.), the conventional method (Conv.), the theoretical upper bound (UB), and the i.i.d. Rayleigh fading (IID). Prop. is the proposed method that optimizes the arrangement by GA in Section III. Conv. is the optimal square arrangement in a fixed environment, and UB is the same as that in Section II. IID is the case where the mean channel capacity of the i.i.d. Rayleigh fading channel is given at each transmitted distance, assuming multipath MIMO transmission.

B. CHARACTERISTICS OF NON-UNIFORM ARRANGEMENT

The evaluation parameters were $M = 3$–16, $D = 1$–100 m (0.1 m increments), and SNR = 20 dB. Except for Fig. 10, SNR was a fixed value without distance attenuation. This is to focus on the influence of the difference in transmission length with regard to the transmitted distances. The GA parameters were empirically set to $G = 50$, $N = 100$, $p_c = 0.8$, $p_m = 0.01$, and 10 elite individuals. In IID, the channels of i.i.d. Rayleigh distribution for 1000 trials were averaged for each transmitted distance.

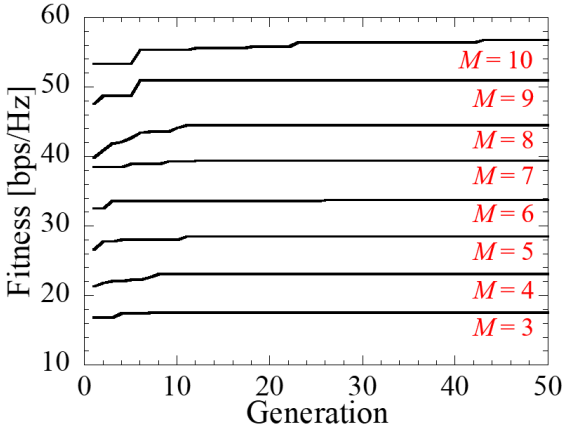

FIGURE 6. Intergenerational transition of maximum fitness.

First, as a confirmation of the operation results of GA, Fig. 6 shows the intergenerational transition of the maximum fitness value when $M = 3$–10. Because the maximum fitness value increases monotonically with the generational change, the approximate optimal solution search by GA functions normally. On the other hand, there is a tendency for many of the elements to converge in less than half of the prescribed generation. In this simulation, the GA parameters are the same regardless of the number of elements for simplification; optimization of parameter settings is a topic for future research.

Fig. 7 shows the approximate optimal solution of each element obtained by GA. The scale of the axis is the same for all elements. When $M = 3, 4, 5$, the shapes were close to equilateral triangles, trapezoids, and regular pentagons, respectively. They were also close to circular arrays. In the calculation condition, a square arrangement range based on (3) and (11) is provided. However, square arrays cannot be created when $M = 3, 5$. On the other hand, a uniform circular array (UCA) may also orthogonalize the propagation

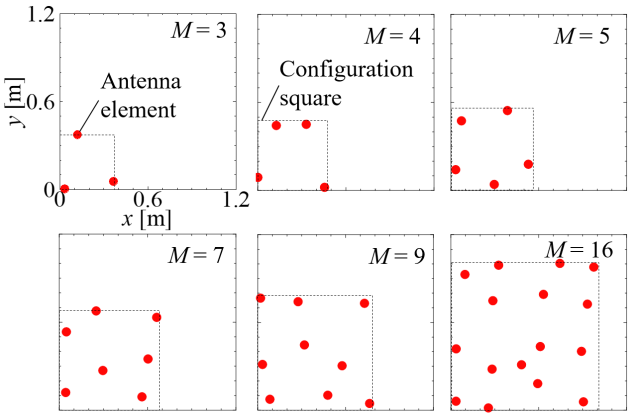

FIGURE 7. Approximate optimal solution.

channels geometrically in a LOS environment [26]. We consider that the optimization was performed while obtaining the antenna aperture area by forming shapes close to circular arrays at $M = 3, 4, 5$. The shapes of $M = 7, 9, 16$ converged to non-uniform until the inside of the arrangement range was reached, whereas this was not observed in the case of $M = 3, 4, 5$. All of them deviated from the shape of UCA or SA. However, the elements were arranged to the inside, as in SA. We consider that the configuration space was efficiently used by increasing the number of elements.

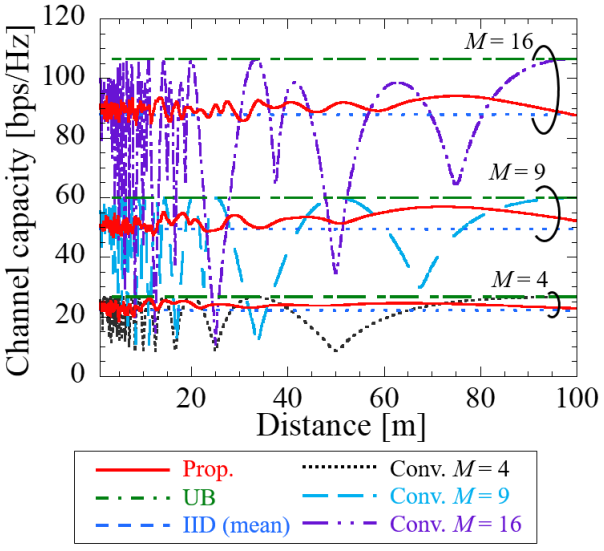

FIGURE 8. Channel capacity versus transmitted distance for $M = 4, 9, 16$.

Fig. 8 shows the channel capacity versus the transmitted distance for $M = 4, 9, 16$. Prop. compensated for the drop in characteristics that occurred in Conv. Table 1 shows the channel capacity mean value (μ), standard deviation (σ), maximum value (Max), minimum value (Min), and spatial correlations at maximum and minimum values (ρ_{Cmax}, ρ_{Cmin}) of Prop. and Conv. in Fig. 8. For the case of three types of elements, Prop. had an increased mean value and a reduced standard deviation when compared with Conv. Although the maximum value of Prop. was inferior to that of Conv., $M = 4, 9, 16$ with Prop. achieved the theoretical upper bounds of 98.0%, 94.9%, and 88.3%, respectively. At the minimum value, Prop. achieved 69.6%, 78.0%, and 79.4% of the theoretical upper bound values of $M = 4, 9, 16$, respectively. The minimum values of Conv. were 32.4%, 16.4%, and 10.1%, respectively, and Prop. yielded improvements of at least 30% owing to the spatial correlation. The maximum values of spatial correlation of Conv. were 1.00. On the other hand, those of Prop. decreased in proportion to the increase in the number of elements. The only factor that changed the spatial correlation under the calculation conditions was the phase difference due to the difference in the transmission length. Therefore, we infer that Prop. optimized the element arrangement and, as a result, the phase difference approached the optimal value and improved the non-orthogonalization of the propagation channel.

TABLE 1. Statistical values for $M = 4, 9, 16$.

Method	Channel capacity [bps/Hz]				ρ	
	μ	σ	Max	Min	C_{max}	C_{min}
Prop. 4 × 4	23.9	0.78	26.1	18.5	0.21	0.69
Conv. 4 × 4	21.8	5.19	26.6	8.64	0.00	1.00
Prop. 9 × 9	53.3	2.40	56.9	46.7	0.19	0.33
Conv. 9 × 9	48.1	12.3	59.9	9.81	0.00	1.00
Prop. 16 × 16	90.7	2.06	94.1	84.6	0.16	0.25
Conv. 16 × 16	84.2	20.8	106.5	10.8	0.00	1.00

From Fig. 8 and Table 1, the mean value and the range of the channel capacity achieved by Prop. gradually approached IID as the number of elements increased. We infer that this is because Prop. created a state close to the uniform phase distribution as observed in a multipath environment by increasing the number of elements in the system. We consider this reason based on a comparison when the number of elements further change. Fig. 9 shows the spatial correlation versus the transmitted distance of Prop. and IID for $M = 3, 4, 5, 7, 9, 16$, where (M, σ) is M: number of elements, and σ: standard deviation of spatial correlation. The results for $M = 3, 4, 5$ and $M = 7, 9, 16$ show visually that the change in the latter value is smaller. Specifically, the standard deviation decreases monotonically in proportion to the increase in the number of elements, except for $M = 9$. From the calculation conditions, the amplitude of the propagation channel of Prop. is constant. From the conditions, when the element arrangement is irregular, the number of patterns of the difference in transmission length increases as the number of elements increases. Therefore, we conclude that Prop. creates a state close to the property of uniform phase distribution in a multipath environment, even for pure LOS.

Finally, we show the results including factors that can actually be assumed (i.e., amplitude components due to difference in transmission length and distance attenuation due to transmitted distance). Fig. 10 shows the channel capacity versus the transmitted distance for $M = 4, 9, 16$. The SNR was set with 10 dB as the reference at $D = 100$ m, and was

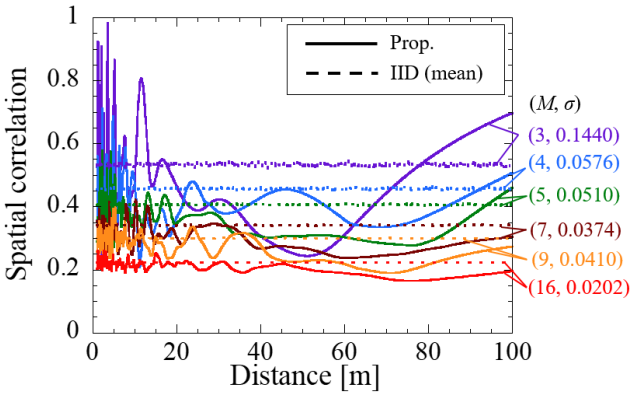

FIGURE 9. Spatial correlation versus transmitted distance for $M = 3, 4, 5, 7, 9, 16$.

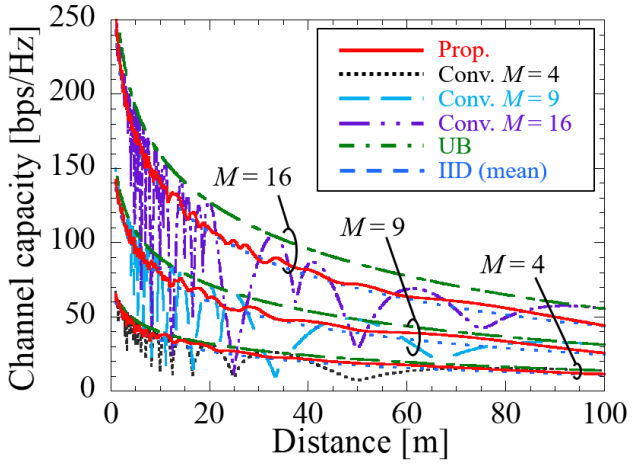

FIGURE 10. Channel capacity versus transmitted distance for $M = 4, 9, 16$ considering distance attenuation.

assigned the distance attenuation proportional to the square of the transmitted distance. Prop. was more effective than Conv. because of the same tendency as that of the result in Fig. 10. From the viewpoint of propagation loss, Fig. 10 also shows that the proposed method was more effective than multipath MIMO transmission. The distance attenuation used for the results of Fig. 10 was a square law. IID requires a multipath environment; thus, it is almost impossible to obtain the characteristics shown in the figure in a real environment.

V. EXPERIMENTAL EVALUATION

A. MEASUREMENT CONDITIONS

In order to confirm the validity of the results in the previous section, we performed a 4 × 4 MIMO transmission experiment outdoors. The main purpose of the experiment was to evaluate the characteristics due to the difference in transmission length formed by the element arrangement, that is, the phase characteristics of the propagation channel. We investigated whether the approximate 2-D non-uniform arrangement was more resistant to changes in the transmitted distance than the uniform arrangement. Table 2 shows the basic evaluation parameters.

TABLE 2. Evaluation parameters.

Center frequency	66.425 GHz
Transmission signal	Continuous-wave
Transmitted distance D	12.8, 17.1, 20, 25.6, 30, 37.8, 50 m
Number of transmitting / receiving elements M	4
Antenna type	Horn antenna
Transmitting / receiving array configuration	Planar array
Array center height	1.65 m

Fig. 11 shows the evaluation equipment. The center frequency is 66.425 GHz. A continuous-wave signal was transmitted because we focused on the phase characteristics dependent on the element arrangement. 4 × 4 MIMO transmission was performed by shifting the signal transmission in time. In order to eliminate the influence of the phase error due to the equipment, the local oscillator was shared for transmission and reception.

Fig. 12 shows the receiving antenna arrangement. The transmitting side had the same configuration and was arranged so as to be symmetrical in the opposite direction of the receiving side. In order to reduce reflection, the jig for installing the antenna was formed in an X shape. Fig. 12(a) shows the approximate optimal arrangement according to the jig when the transmitted distance is set to 1–50 m (0.1 m increments) using the GA algorithm introduced in Section III, where the GA parameters are the same as those in the previous section. Fig. 12(b) shows a uniform arrangement with an element feeding point spacing of 0.34 m. In Fig. 12(b), the maximum characteristics are achieved near a transmitted distance of 50 m. In the previous section, the evaluation was performed using an omnidirectional antenna element. In the experiment, a horn antenna with a 3-dB beam width of 20° was used in both the horizontal and vertical directions in order to realize transmission at a center frequency of 66.425 GHz. Therefore, we set the evaluation interval of the experiment within the interval where the characteristic of LOS-MIMO is obtained when the directivity is approximated using a cosine pattern. When the 3-dB beam width is θ_{BW}, the antenna response due to directivity at the angle θ is calculated as [27]

$$F_{\theta_{BW}}(\theta) = \cos^n(\theta) \tag{13}$$

with

$$\cos^n\left(\frac{\theta_{BW}}{2}\right) = \frac{1}{\sqrt{2}} \tag{14}$$

$$n = -\frac{1}{2\log_2\left\{\cos\left(\frac{\theta_{BW}}{2}\right)\right\}}. \tag{15}$$

Fig. 13 shows the simulation value of the channel capacity versus the transmitted distance when the antenna response of (13) is considered in the antenna arrangement of Fig. 12. The SNR was given considering distance attenuation proportional to the square of the transmitted distance. Even when the 3-dB beam width was 20°, the tendency was the same as that in Section IV. Therefore, we evaluated at 12.8, 17.1, 20, 25.6,

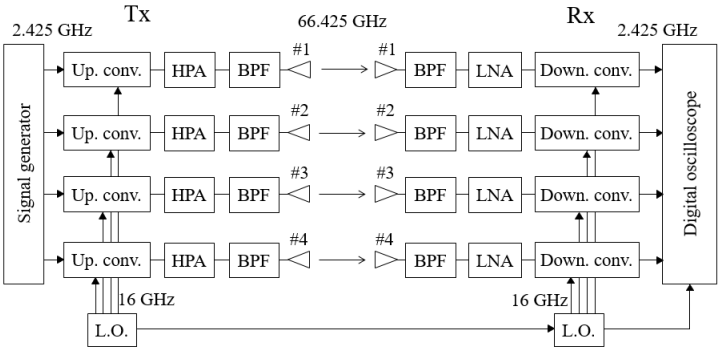

Up. conv. : up converter, L.O.: local oscillator, HPA: high power amplifier, BPF: band-pass filter, LNA: low noise amplifier, Down. conv.: down converter.

(a) Block diagram

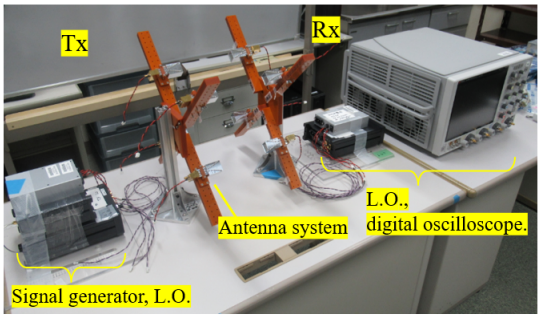

(b) Actual equipment image

FIGURE 11. Evaluation equipment.

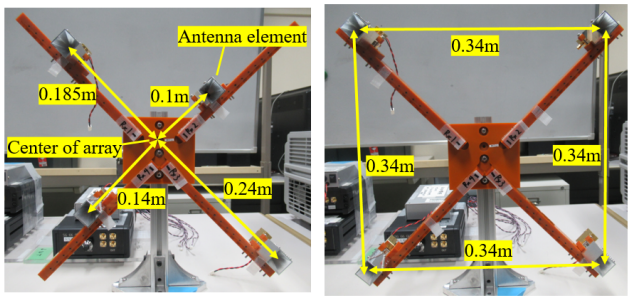

(a) Prop. (b) Conv.

FIGURE 12. Antenna arrangement.

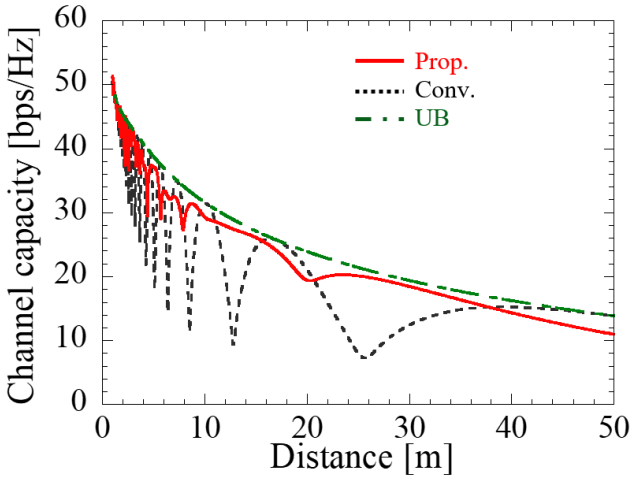

FIGURE 13. Channel capacity versus transmitted distance when the directivity of a 3-dB beam width of 20° is considered.

30, 37.8, and 50 m, where the characteristics of both Prop. and Conv. are prominent.

Fig. 14 shows the measurement environment. The location was a straight road with a LOS between the Faculty of Engineering Building and the Information Science and Technology Building at Niigata University in Japan. Although we

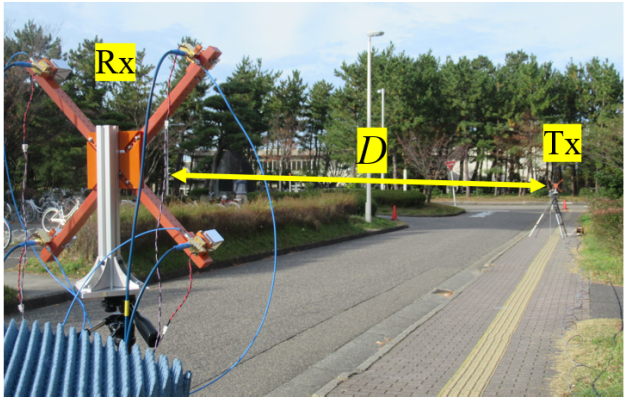

FIGURE 14. Measurement environment.

did not use UAVs in this measurement, it was set up so that an environment close to pure LOS could be realized by providing an antenna position that could secure the first Fresnel zone [27] at 66.425 GHz. As a measurement method, the model is the same as that in Fig. 2. Tx and Rx face each other, and Tx is moved in parallel in the transmission direction, considering the ease of equipment movement. In Section IV, Rx is moved in parallel. Note that if there is no movement in the *xy* direction, it is evident that the channel characteristics are the same regardless of whether Tx or Rx is moved in parallel.

B. EXPERIMENTAL RESULTS

Fig. 15 shows the eigenvalue versus the transmitted distance, where Simu. is the simulation value, and Meas. is the measured value. The simulation value is a characteristic derived from the propagation channel using (1). Both the simulation value and the measured value were normalized to the magnitude of the amplitude as unity. The SNR was assigned considering distance attenuation proportional to the square of the transmitted distance. In Fig. 15(a), all the eigenvalues of the measured values at each measurement point

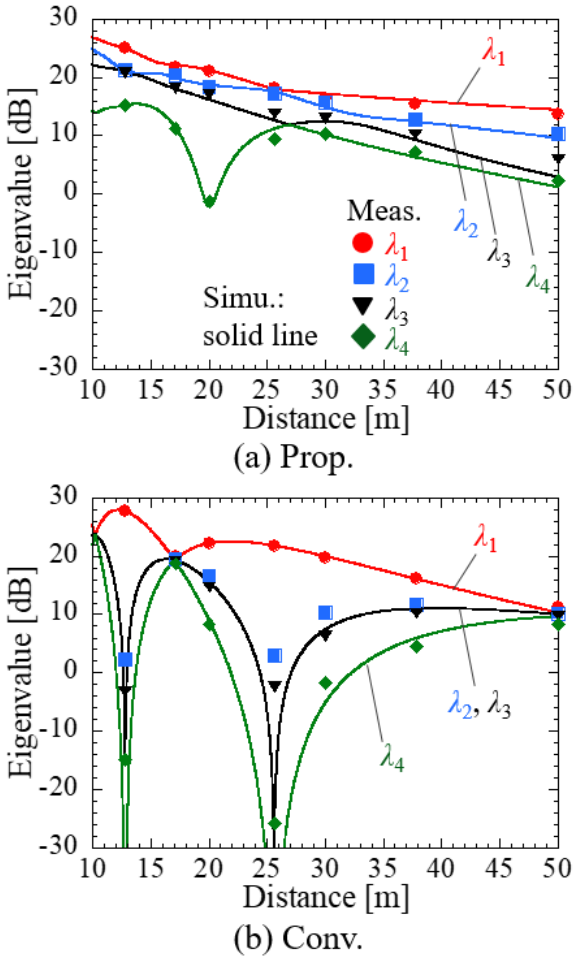

FIGURE 15. Eigenvalue versus transmitted distance. Simulated values are calculated using direct waves only.

almost coincided with the simulation values. In Fig. 15(b), the eigenvalues approach a constant value at 17.1 m and 50 m, where the difference in transmission length is an odd multiple of 1/4 wavelength. At 12.8 m and 25.6 m, where the difference in transmission length is an even multiple of 1/4 wavelength, degeneracy other than that of the first eigenvalue was observed. In addition, a relationship of $\lambda_2 \approx \lambda_3$ was observed. Theoretically, when 4×4 square arrays face each other, the two elements other than the opposite element and the diagonal element have the same difference in transmission length. This similar tendency was obtained in the measured values. Therefore, it was clarified by this measurement that the phase characteristics of 4×4 LOS-MIMO at 66.425 GHz can be realized in a real environment in both uniform and non-uniform arrangements.

Fig. 15 shows that the eigenvalue distribution is improved by the element arrangement, even with the measured values; however, errors from the simulation values also appear. Therefore, we discuss the reliability of the experimental results, including the possible error factors in this measurement. The main errors that can be considered in this measurement are misalignment of the transmitter and receiver positions, and the multipath environment. First, regarding the misalignment of the positions, in the 2×2 LOS-MIMO, although it is a uniform arrangement, it has been reported that the change in channel capacity characteristics is approximately 1% even if the transmitter/receiver array deviates approximately 20% horizontally and vertically from the facing position, and approximately 30° from the broadside direction to the endfire direction [2]. Therefore, because it is possible to guarantee a certain level of robustness even when the positions are misaligned, misalignment of the positions is expected to be a small error factor when compared with multipath. Based on this point, we focus on the error in Fig. 15(a). The error between the measured value and the simulated value in Fig. 15(a) is as small as approximately 3 dB at maximum, which is small compared with that in 15(b). The fact that the influence of topography and wind was not completely eliminated in this measurement, is considered to have affected the error in Fig. 15(a).

Next, we argue that the effects of multipath appear in the error in Fig. 15(b). We consider that multipath causes λ_2 and λ_3 to be slightly different and a particularly large error is found in λ_4. As shown in Fig. 14, the measurement environment is ground communication; therefore, it is expected that multipath exists even though the LOS is secured. Fig. 16 shows the eigenvalue versus the transmitted distance by comparing the measured value with the simulation value considering Nakagami–Rician fading. The propagation channel of the simulation value is given by [10]

$$\boldsymbol{H} = \sqrt{\frac{K}{1+K}}\boldsymbol{H}_{LOS} + \sqrt{\frac{1}{1+K}}\boldsymbol{H}_{NLOS}, \tag{16}$$

where K is the Rician factor; $\boldsymbol{H}_{LOS}$ is the direct wave component according to (1); and $\boldsymbol{H}_{NLOS}$ indicates a multipath component. In Fig. 16, $K = 20$ dB, and $\boldsymbol{H}_{NLOS}$ was obtained by averaging the propagation channels that follow the i.i.d. Rayleigh fading generated 1000 times. Fig. 16(a) illustrates the case of a non-uniform arrangement. There is no significant change from the numerical relationship of the results in Fig 15(a). It is evident that the eigenvalue distribution decreases monotonically regardless of the distance as K is brought closer to 0 dB. Therefore, we reconsider that the decrease in $\boldsymbol{H}_{LOS}$ is not the main component of the error in the non-uniform arrangement. On the other hand, as shown in Fig. 16(b), the decrease in $\boldsymbol{H}_{LOS}$ is a persuasive factor for the error in the uniform arrangement. Fig. 16(b) shows that the measured and simulated values tend to be closer than the results of Fig. 15(b). In particular, this tendency is prominent at λ_2–λ_4 at 12.8 m and 25.6 m. In addition, there was a slight difference between λ_2 and λ_3 at each measurement point by giving $\boldsymbol{H}_{NLOS}$, and it is explainable that λ_2 and λ_3, which should theoretically match, did not match in the measured values. From the above, we conclude that the power ratio of approximately $K = 20$ dB between $\boldsymbol{H}_{LOS}$ and $\boldsymbol{H}_{NLOS}$ was one of the causes of error in Fig. 15. In this regard, we consider that characteristics closer to simulation values can be obtained than the measured values of this experiment when

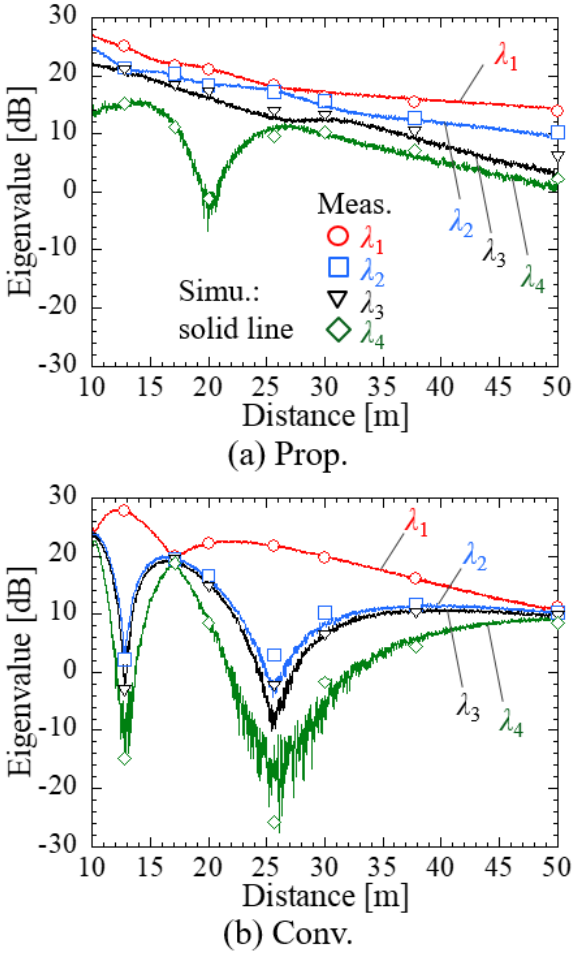

FIGURE 16. Eigenvalue versus transmitted distance. Simulated values are calculated using Nakagami–Rician fading. $K = 20$ dB.

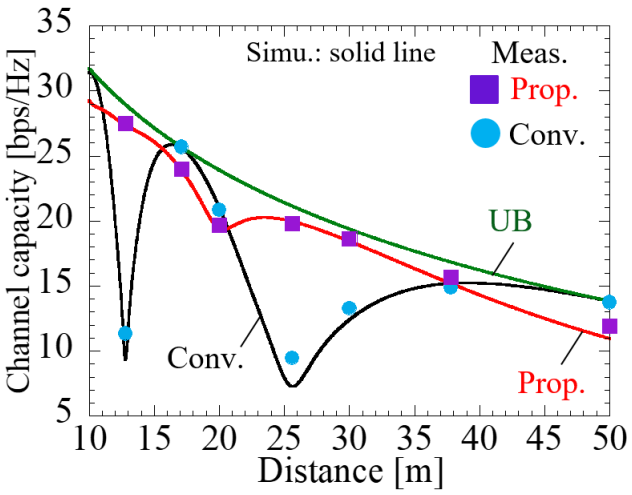

FIGURE 17. Channel capacity versus transmitted distance. Simulated values are calculated using direct waves only.

air communication is performed using UAVs. This is because the effects of multipath are reduced and in the 60-GHz band, there is less interference from existing systems. This measurement result also means that a phase characteristic close to the simulation value can be obtained even in an environment with multipath. This suggests that LOS-MIMO transmission is possible even if UAVs are placed in a low place. In the future, we plan to verify this by experiments using UAVs.

Finally, Fig. 17 shows the channel capacity versus the transmitted distance. As in Fig. 15, the propagation channel of the simulation value was calculated by (1). Both the simulation value and the measured value were normalized to the magnitude of the amplitude as unity. The SNR was assigned considering distance attenuation proportional to the square of the transmitted distance. In the uniform arrangement, the theoretical upper limit was achieved at 17.1 m and 50 m, and the characteristics deteriorated significantly at 12.8 m and 25.6 m. As discussed thus far, $K = 20$ dB and $\boldsymbol{H}_{LOS}$ was superior to $\boldsymbol{H}_{NLOS}$; therefore, the phase characteristics of LOS-MIMO appeared in the actual environment. This result means that the channel capacity characteristic of the conventional uniform arrangement depends on the change in the transmitted distance even in the real environment. On the other hand, the channel capacity characteristics of the non-uniform arrangement also showed the same tendency as the simulation values. Therefore, we clarify that even in a real environment, the LOS-MIMO system proposed in this study, with a 2-D non-uniform element arrangement, is resistant to changes in the transmitted distance with only a fixed element arrangement.

VI. CONCLUSION

This study examined the antenna configuration of LOS-MIMO transmission independent of the transmitted distance. Focusing on the geometrical relationship between the antenna element arrangement and the transmitted distance, we proposed a 2-D fixed element arrangement using GA. We showed the effectiveness of the proposed method by evaluating the channel capacity characteristics with respect to transmitted distances. In the proposed method, the element position of each individual was updated for each generation using a genetic operator. The approximate optimum element arrangement was determined within the given element arrangement range and the transmitted distance range. When the number of elements was 4, 9, and 16, the proposed method improved the mean value and the standard deviation of the channel capacity when compared with the conventional square LOS-MIMO transmission. The spatial correlation characteristics in the proposed method tended to converge in proportion to the increase in the number of elements, and the characteristics close to multipath MIMO transmission were realized in the LOS environment. We evaluated the validity of this study by experimenting with a 4×4 LOS-MIMO transmission in an actual environment. As a result of the experiment, we clarified that the same tendency was obtained for both the simulation value and the actual measurement value. Future research on this topic includes a derivation of the strict optimal solution for a 2-D

fixed antenna element arrangement, an approximate optimization including deviation from the opposite position of the transmitting and receiving antennas, and an experimental evaluation using UAVs with suitable hardware. Finally, In this study, we focused on UAVs, which have been studied for use as communication systems in recent years, and proposed a LOS-MIMO system that considers the mobility of UAVs. The new LOS-MIMO system, which is different from the conventional fixed communication, is expected to be applied to wireless systems other than the UAV communication, and this is one of the future research items. Moreover, this technology can be applied not only transmission with a big data between UAVs but also the transmission of the estimation results of radio sources with direction of arrival estimation in LOS environment, and so on.

REFERENCES

[1] M. Shafi, A. F. Molisch, P. J. Smith, T. Haustein, P. Zhu, P. De Silva, F. Tufvesson, A. Benjebbour, and G. Wunder, "5G: A tutorial overview of standards, trials, challenges, deployment, and practice," *IEEE J. Sel. Areas Commun.*, vol. 35, no. 6, pp. 1201–1221, Jun. 2017.

[2] I. Sarris and A. R. Nix, "Design and performance assessment of high-capacity MIMO architectures in the presence of a line-of-sight component," *IEEE Trans. Veh. Technol.*, vol. 56, no. 4, pp. 2194–2202, Jul. 2007.

[3] F. Bohagen, P. Orten, and G. Oien, "Optimal design of uniform rectangular antenna arrays for strong line-of-sight MIMO channels," *EURASIP J. Wireless Commun. Netw.*, vol. 2007, Aug. 2007, Art. no. 045084, doi: 10.1155/2007/45084.

[4] C. Sheldon, E. Torkildson, M. Seo, C. Yue, U. Madhow, and M. Rodwell, "A 60 GHz line-of-sight 2×2 MIMO link operating at 1.2 Gbps," in *Proc. IEEE Antennas Propag. Soc. Int. Symp.*, Jul. 2008, doi: 10.1109/aps.2008.4619161.

[5] S. M. Mohammadi, L. K. S. Daldorff, J. E. S. Bergman, R. L. Karlsson, B. Thide, K. Forozesh, T. D. Carozzi, and B. Isham, "Orbital angular momentum in radio—A system study," *IEEE Trans. Antennas Propag.*, vol. 58, no. 2, pp. 565–572, Feb. 2010.

[6] D. Lee, H. Sasaki, H. Fukumoto, K. Hiraga, and T. Nakagawa, "Orbital angular momentum (OAM) multiplexing: An enabler of a new era of wireless communications," *IEICE Trans. Commun.*, vol. E100.B, no. 7, pp. 1044–1063, 2017.

[7] S. Saito, H. Suganuma, K. Ogawa, and F. Maehara, "Influence of the number of uniform circular arrays on system capacity in OAM multiplexing," in *Proc. 21st Int. Symp. Wireless Pers. Multimedia Commun. (WPMC)*, Nov. 2018, doi: 10.1109/wpmc.2018.8712929.

[8] Y. Karasawa, "Innovative antennas and propagation studies for MIMO systems," *IEICE Trans. Commun.*, vols. E90-B, no. 9, pp. 2194–2202, Sep. 2007.

[9] S. Jayaweera and H. Poor, "On the capacity of multiple-antenna systems in Rician fading," *IEEE Trans. Wireless Commun.*, vol. 4, no. 3, pp. 1102–1111, May 2005.

[10] A. Paulaj, R. Nabar, and D. Gore, *Introduction to Space-Time Wireless Communications*. New York, NY, USA: Cambridge Univ. Press, 2008.

[11] J. Edstam, J. Hansryd, S. Carpenter, T. Emanuelsson, Y. Li, and H. Zirath, "Microwave backhaul evolution—Reaching beyond 100 GHz," *Ericsson Technol. Rev.*, vol. 2, pp. 1–15, Feb. 2017. [Online]. Available: https://www.ericsson.com/en/reports-and-papers/ericsson-technology-review/articles/microwave-backhaul-evolution-reaching-beyond-100ghz

[12] Y. Zeng, R. Zhang, and T. J. Lim, "Wireless communications with unmanned aerial vehicles: Opportunities and challenges," *IEEE Commun. Mag.*, vol. 54, no. 5, pp. 36–42, May 2016.

[13] M. Bucur, T. Sorensen, R. Amorim, M. Lopez, I. Z. Kovacs, and P. Mogensen, "Validation of large-scale propagation characteristics for UAVs within urban environment," in *Proc. IEEE 90th Veh. Technol. Conf. (VTC-Fall)*, Sep. 2019, doi: 10.1109/vtcfall.2019.8891422.

[14] "Guidelines for evaluation of radio interface technologies for IMT-advanced," Int. Telecommun. Union, Geneva, Switzerland, Tech. Rep. ITU 1–2135, Dec. 2009.

[15] P. Zhou, X. Fang, Y. Fang, R. He, Y. Long, and G. Huang, "Beam management and self-healing for mmWave UAV mesh networks," *IEEE Trans. Veh. Technol.*, vol. 68, no. 2, pp. 1718–1732, Feb. 2019.

[16] Z. Xiao, P. Xia, and X.-G. Xia, "Enabling UAV cellular with millimeter-wave communication: Potentials and approaches," *IEEE Commun. Mag.*, vol. 54, no. 5, pp. 66–73, May 2016.

[17] E. Torkildson, C. Sheldon, U. Madhow, and M. Rodwell, "Nonuniform array design for robust millimeter-wave MIMO links," in *Proc. IEEE Global Telecommun. Conf. (GLOBECOM)*, Nov. 2009.

[18] P. Wang, Y. Li, Y. Peng, S. C. Liew, and B. Vucetic, "Non-uniform linear antenna array design and optimization for millimeter-wave communications," *IEEE Trans. Wireless Commun.*, vol. 15, no. 11, pp. 7343–7356, Nov. 2016.

[19] A. A. Glazunov, N. Amani, A. U. Zaman, M. V. Ivashina, and R. Maaskant, "Capacity gains of (3 × 3)×(3 × 3) MIMO fixed links with planar aperiodic sparse arrays in pure-LOS channels," in *Proc. IEEE-APS Topical Conf. Antennas Propag. Wireless Commun. (APWC)*, Sep. 2018, doi: 10.1109/apwc.2018.8503781.

[20] D. E. Goldberg, *Genetic Algorithms in Search, Optimization and Machine Learning*. Boston, MA, USA: Addison-Wesley, 1989.

[21] T. Maruyama and T. Hori, "Vector evaluated GA-ICT for novel optimum design method of arbitrarily arranged wire grid model antenna and application of GA-ICT to sector-antenna downsizing problem," *IEICE Trans. Commun.*, vols. E84-B, no. 11, pp. 3014–3022, Nov. 2001.

[22] S. Baluja and R. Caruana, "Removing the genetics from the standard genetic algorithm," in *Proc. 12th Int. Conf. Mach. Learn.*, 1995, pp. 38–46.

[23] J. E. Baker, "Adaptive selection methods for genetic algorithms," in *Proc. 1st Int. Conf. Genetic Algorithms Appl.* Hillsdale, NJ, USA: Lawrence Erlbaum Associates, 1985, pp. 101–111.

[24] N. Matsumura, K. Nishimori, R. Taniguchi, T. Mitsui, and T. Hiraguri, "Effect of propagation environment control method using drone MIMO relay station," in *Proc. Int. Symp. Antennas Propag. (ISAP)*, Oct. 2018, Paper WeC2-6.

[25] K. Nishimori, N. Honma, T. Seki, and K. Hiraga, "On the transmission method for short-range MIMO communication," *IEEE Trans. Veh. Technol.*, vol. 60, no. 3, pp. 1247–1251, Mar. 2011.

[26] G. D. Surabhi and A. Chockalingam, "Efficient signaling schemes for mmWave LOS MIMO communication using uniform linear and circular arrays," in *Proc. IEEE 85th Veh. Technol. Conf. (VTC Spring)*, Jun. 2017, doi: 10.1109/vtcspring.2017.8108379.

[27] T. A. Milligan, *Modern Antenna Design*, 2nd ed. Hoboken, NJ, USA: Wiley, 2005.

NAOKI MATSUMURA (Student Member, IEEE) received the B.E. degree from the Faculty of Engineering, Niigata University, Niigata, Japan, in 2018, where he is currently pursuing the M.E. degree with the Graduate School of Science and Technology. His research interests are MIMO antenna systems for 5G and its beyond.

KENTARO NISHIMORI (Member, IEEE) received the B.E., M.E., and Ph.D. degrees in electrical and computer engineering from the Nagoya Institute of Technology, Nagoya, Japan, in 1994, 1996, and 2003, respectively. In 1996, he joined the NTT Wireless Systems Laboratories, Nippon Telegraph and Telephone Corporation, Japan. He was a Visiting Researcher with Aalborg University, Aalborg, Denmark, from February 2006 to January 2007. He has been an Associate Professor with Niigata University, since 2009, where he is currently a Research Professor. His main interests are spatial signal processing, including massive MIMO systems. He is a Senior Member of IEICE. He received the Young Engineers Award from the IEICE of Japan, in 2001, the Young Engineer Award from IEEE AP-S Japan Chapter, in 2001, and the IEICE Best Paper Award, in 2010.

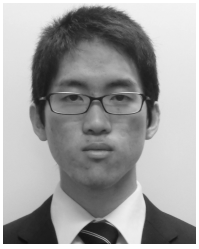

RYOTARO TANIGUCHI (Student Member, IEEE) received the B.E. and M.E. degrees from Niigata University, Niigata, Japan, in 2016 and 2018, respectively, where he is currently pursuing the Ph.D. degree with the Graduate School of Science and Technology. His research interests include massive MIMO system and millimeter wave propagation.

TAKEFUMI HIRAGURI (Member, IEEE) received the M.E. and Ph.D. degrees from the University of Tsukuba, Ibaraki, Japan, in 1999 and 2008, respectively. In 1999, he joined the NTT Access Network Service Systems Laboratories, Nippon Telegraph and Telephone Corporation, Japan. He has been involved in research and development of MAC protocol for the high speed and the high communication quality in wireless systems. He is currently a Professor with the Nippon Institute of Technology. He is a Senior Member of IEICE.

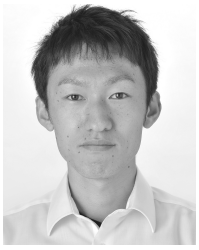

TAKASHI TOMURA (Member, IEEE) received the B.S., M.S., and D.E. degrees in electrical and electronic engineering from the Tokyo Institute of Technology, Tokyo, Japan, in 2008, 2011, and 2014, respectively.

He was a Research Fellow of the Japan Society for the Promotion of Science (JSPS), in 2013. From 2014 to 2017, he was with Mitsubishi Electric Corporation, Tokyo, and was involved in research and development of aperture antennas for satellite communications and radar systems. From 2017 to 2019, he was a Specially Appointed Assistant Professor with the Tokyo Institute of Technology, Tokyo, where he is currently an Assistant Professor. His research interests include electromagnetic analysis, aperture antennas, and planar waveguide slot array antennas. Dr. Tomura is a member of the IEICE. He received the Best Student Award from Ericsson, Japan, in 2012, the IEEE AP-S Tokyo Chapter Young Engineer Award, in 2015, and the Young Researcher Award from IEICE Technical Committee on Antennas and Propagation, in 2018.

JIRO HIROKAWA (Fellow, IEEE) received the B.S., M.S., and D.E. degrees in electrical and electronic engineering from the Tokyo Institute of Technology (Tokyo Tech), Tokyo, Japan, in 1988, 1990, and 1994, respectively. He was a Research Associate with Tokyo Tech, from 1990 to 1996, and an Associate Professor with Tokyo Tech, from 1996 to 2015, where he is currently a Professor. He was with the Antenna Group of Chalmers University of Technology, Gothenburg, Sweden, as a Postdoctoral Fellow, from 1994 to 1995. His research area has been in slotted waveguide array antennas and millimeter-wave antennas. He is a Fellow of IEICE. He received the IEEE AP-S Tokyo Chapter Young Engineer Award, in 1991, the Young Engineer Award from IEICE, in 1996, the Tokyo Tech Award for Challenging Research, in 2003, Young Scientists' Prize from the Minister of Education, Cultures, Sports, Science and Technology in Japan, in 2005, the Best Paper Award, in 2007, the Best Letter Award from IEICE Communications Society, in 2009, and the IEICE Best Paper Award, in 2016 and 2018.